BIOCHEMISTRY
including biophysical chemistry & molecular biology

Article

pubs.acs.org/biochemistry

Energetics of Protein Stability at Extreme Environmental Temperatures in Bacterial Trigger Factors

Caroline Struvay,[†] Sonia Negro,[†] André Matagne,[‡] and Georges Feller*[,†]

[†]Laboratory of Biochemistry and [‡]Laboratory of Enzymology and Protein Folding, Center for Protein Engineering, University of Liège, B-4000 Liège-Sart Tilman, Belgium

Supporting Information

ABSTRACT: Trigger factor is the first molecular chaperone interacting cotranslationally with virtually all nascent polypeptides synthesized by the ribosome in bacteria. The stability of this primary folding assistant was investigated using trigger factors from the Antarctic psychrophile *Pseudoalteromonas haloplanktis*, the mesophile *Escherichia coli*, and the hyperthermophile *Thermotoga maritima*. This series covers nearly all temperatures encountered by living organisms. We show that proteins adapt their stability over the whole range of biological temperatures via adjustments of the same fundamental mechanisms, involving increases in enthalpic stabilization and decreases in unfolding rates, in parallel with the environmental temperature. Enthalpic stabilization in trigger factors is characterized by large increases in the melting temperature, T_m, ranging from 33 to 96.6 °C, associated with similarly large increases in unfolding enthalpy as revealed by differential scanning calorimetry. Stopped-flow spectroscopy shows that the folding rate constants for the three investigated proteins are similar, whereas the unfolding rate constants differ by several orders of magnitude, revealing that kinetic resistance to unfolding drives adjustments of protein stability. While the unusual stability of hyperthermophilic proteins has attracted much attention, this study indicates that they are an extreme case of a more general continuum, the other extreme being represented by natively unstable proteins from psychrophiles.

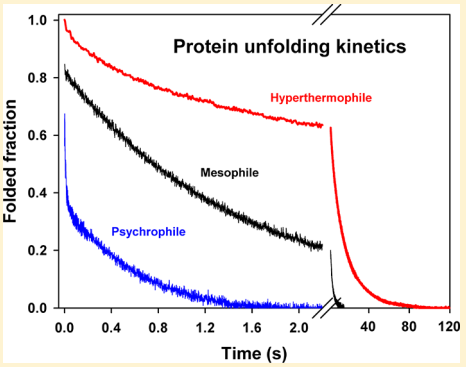

Extreme environments, previously regarded as abiotic, have revealed astonishing biodiversity and have also demonstrated the outstanding adaptability of the microbial world to harsh physicochemical conditions.[1,2] As far as temperature is concerned, hyperthermophiles thriving in hot springs, solfatares, and hydrothermal vents have pushed the upper temperature for life to 122 °C, as exemplified by the Archeon *Methanopyrus kandleri*.[3] At the other extreme of the biological temperature scale, psychrophiles (i.e., cold-loving microorganisms) live permanently at temperatures close to the freezing point of water and even at sub-zero temperatures.[4−6] The detection of metabolically active bacteria at −20 °C in the brine veins between sea ice crystals[7] illustrates the unsuspected capacity of psychrophiles to adapt to low temperatures. Microbial life at these extreme biological temperatures obviously requires a vast array of adaptations at all cellular levels. However, a key determinant of these adaptations lies in the protein function that drives microbial metabolism and the cell cycle. Hyperthermophilic proteins are the most thermostable biological macromolecules but become inactive at room temperature as a result of their rigid structure. By contrast, psychrophilic proteins are heat-labile and very unstable as a consequence of their improved structural flexibility required for function at low temperatures.[4,8] Crystal and nuclear magnetic resonance structures of these extremophilic proteins have revealed a striking continuum in the adaptive strategies aimed at adjusting protein stability to environmental temperatures. In psychrophiles, all structural factors, weak interactions, and hydrophobic effects currently known to stabilize proteins are drastically reduced in strength and number,[4,8,9] while the same factors are improved in thermophilic and hyperthermophilic proteins.[10−12]

Besides the static picture provided by three-dimensional structures, protein stability in solution is an exquisite balance among several, sometimes opposing, contributions. Thermodynamic stability is quantitatively described by the Gibbs free energy changes upon unfolding, ΔG°_{NU}, determined by equilibrium unfolding and differential scanning calorimetry (DSC). Furthermore, in a simple two-state process between the native (N) and unfolded (U) states, the equilibrium constant K_{NU} is merely expressed as the k_{NU}/k_{UN} ratio of the kinetic constants for unfolding and refolding, as measured by stopped-flow methods. Thermodynamic and kinetic contributions are therefore both involved in protein stability. Thermodynamic and kinetic data available for hyperthermophilic proteins show that unfolding is dramatically slower than in mesophilic proteins. This suggests that kinetic resistance to unfolding is linked to hyperstability.[13,14] By contrast, kinetic data are lacking for psychrophilic proteins, and only one comprehensive microcalorimetric study has been reported for a cold-adapted α-amylase.[15] As a result, several basic questions remain to be

Received: February 25, 2013
Revised: March 25, 2013
Published: April 2, 2013

answered. What are the fundamental mechanisms allowing adaptation of protein stability in the whole range of biological temperatures? Are there mechanisms specific to extremely high temperatures and others to extremely low temperatures? In a biophysical context, what are the thermodynamic and kinetic contributions to protein stability in the temperature range where life occurs? These questions prompted us to analyze the stability of homologous trigger factors (TFs) from the Antarctic psychrophile *Pseudoalteromonas haloplanktis* (*Ph*TF), the mesophile *Escherichia coli* (*Ec*TF), and the hyperthermophile *Thermotoga maritima* (*Tm*TF). This series covers nearly all temperatures encountered by living organisms. TF is the first molecular chaperone interacting cotranslationally with virtually all newly synthesized polypeptides by the ribosome. It delays premature chain compaction and maintains the elongating polypeptide in a nonaggregated state until sufficient structural information for productive folding is available and subsequently promotes protein folding.[16−18] The role of TF in cold adaptation[19] and its pivotal function as a folding assistant in all bacteria guided our selection of this chaperone for stability studies. We show here that these proteins adapt their stability over the whole range of biological temperatures via adjustments of the same fundamental mechanisms.

MATERIALS AND METHODS

Gene Cloning, Protein Production, and Purification. *Ph*TF and *Ec*TF genes have been previously amplified via polymerase chain reaction from genomic DNA of *P. haloplanktis* TAC 125 and *E. coli* RR1, respectively, and cloned into the pET22b expression vector (Novagen). Both proteins were produced and purified as described previously.[19] The *Tm*TF gene was amplified from *T. maritima* DSM3109 genomic DNA using primers designed to introduce an NdeI site overlapping the initiation codon and a BamHI site after the stop codon (forward, 5′-ggatgaacacatatggaagtgaaggagctt-3′; reverse, 5′-atgggaacgggatcctcaattatcttcttttccttc-3′), allowing cloning at the corresponding sites of pET22b. Recombinant *Tm*TF was expressed in *E. coli* BL21(DE3) and purified as described previously[19] with the following modifications. Chromatography on Phenyl-Sepharose CL-4B was performed in 35 mM Hepes, 10% saturation in $(NH_4)_2SO_4$, and 1 mM PMSF (pH 7.6), and proteins were eluted with a decreasing gradient from 10 to 0% saturation in $(NH_4)_2SO_4$. An additional purification step was performed by size exclusion chromatography on a Sephacryl S-100-HR column (3 cm × 90 cm) equilibrated in 35 mM Hepes, 250 mM NaCl, and 1 mM PMSF (pH 7.6). Purified protein samples (∼3 mg/mL) were stored at −70 °C.

Differential Scanning Calorimetry. Measurements under standard conditions were performed using a MicroCal VP-DSC instrument at a scan rate of 60 K/h under ∼25 psi positive cell pressure. Samples (∼2−3 mg/mL) were dialyzed overnight against 30 mM Mops and 250 mM NaCl (pH 7.6). Reference baselines were recorded using dialysis buffer. For *Tm*TF, both the sample and the reference buffer were brought to 1 M 3-(1-pyridinio)-1-propanesulfonate (i.e., a nondetergent sulfobetaine) as detailed previously.[20] After cell loading, the protein concentration was determined for the remaining sample by the bicinchoninic method (Pierce). Thermograms were analyzed according to a non-two-state model in which the melting point (T_m), the calorimetric enthalpy (ΔH_{cal}), and the van't Hoff enthalpy (ΔH_{eff}) of individual transitions are fit independently using MicroCal Origin version 7.

GdmCl-Induced Unfolding Transitions. Equilibrium unfolding was followed by changes in intrinsic fluorescence, using a JASCO FP-8300 spectrofluorometer at an excitation wavelength of 280 nm, emission wavelengths of 307 and 335 nm, and protein concentrations of 100 μg/mL. Unfolding was monitored at selected temperatures after overnight incubation of the samples at various GdmCl concentrations in 30 mM Hepes and 250 mM NaCl (pH 7.6). Denaturant concentrations were determined from refractive index measurements using a R5000 Atago hand refractometer.[21] Reversible equilibrium unfolding curves of *Ph*TF were analyzed on the basis of a two-state model as described previously,[22−24] whereas *Ec*TF and *Tm*TF were analyzed on the basis of a three-state model:[25−28]

$$y_{obs} = [y_N + p[D] + \exp(a)y_I + \exp(a+b)(y_U + q[D])] / [1 + \exp(a) + \exp(a+b)] \quad (1)$$

$$\text{with } a = -[\Delta G^\circ(H_2O)_{NI} + m_{NI}[D]]/(RT)$$

$$\text{and } b = -[\Delta G^\circ(H_2O)_{IU} + m_{IU}[D]]/(RT)$$

where y_{obs} is the measured fluorescence at GdmCl concentration [D]; y_N, y_I, and y_U are the signals for the N, I, and U states, respectively; m_{NI} and m_{IU} are the slopes of the respective transitions; $\Delta G^\circ(H_2O)_{NI}$ and $\Delta G^\circ(H_2O)_{IU}$ are the free energy changes of the respective transitions at 0 M GdmCl; and p and q are the slopes of the native and denatured baselines, respectively.

Kinetics of Unfolding and Refolding. All experiments were performed in 30 mM Hepes and 250 mM NaCl (pH 7.6) using a final protein concentration of 0.1 mg/mL (∼2 μM). To initiate refolding reactions, psychrophilic, mesophilic, and thermophilic TFs (1 mg/mL) unfolded for 24 h in 1, 2, and 4 M GdmCl, respectively, were diluted 10-fold with aqueous buffer or with GdmCl solutions of varying concentrations to give the desired final concentrations of GdmCl. Conversely, unfolding reactions were initiated by a 10-fold dilution of native TFs with the same buffer containing various amounts of GdmCl, to yield the final concentrations. Fast kinetic experiments were performed at 20 °C using a Bio-Logic (Claix, France) SFM-3 stopped-flow apparatus, coupled with a MOS-200 spectrophotometer and a MPS-51 power supply. Fluorescence measurements were performed using a 1.5 mm path length cell (FC-15). The dead time of the apparatus was found to be ∼10 ms under all experimental settings: this value was estimated by monitoring the fluorescence of the reduction of dichlorophenolindophenol by ascorbic acid, as described by the manufacturer. Unfolding and refolding kinetics were followed by intrinsic fluorescence with an excitation wavelength of 280 nm, and total emission above 320 nm was monitored using a high-pass filter. Kinetic traces resulted from the accumulation of five identical experiments. All kinetic data were analyzed according to a sum of exponentials:

$$y_t = y_\infty + \sum_{n=1}^{i} A_i \exp(-k_i t) \quad (2)$$

where y_t is the intensity of the fluorescence at time t, y_∞ is the signal value for an infinite time, and A is the amplitude of the signal associated with rate constant k. The data sets were averaged to obtain the rate constant, and errors were calculated as standard deviations.

dx.doi.org/10.1021/bi4002387 | *Biochemistry* 2013, 52, 2982−2990

Table 1. General Properties of the Investigated Trigger Factors

protein	source	T_{env}[a] (°C)	GenBank entry	no. of residues	M_r (Da)	no. of Trp's	no. of Tyr's	PDB entry
*Ph*TF	*P. haloplanktis* TAC125	<0	CR954246.1	434	47534.5	1	6	–
*Ec*TF	*E. coli* RR1	37	M34066.1	432	48192.6	1	8	1W26
*Tm*TF	*T. maritima* DSM3109	85–90	EHA61365.1	425	49897.7	2	14	3GUO

[a]Estimated average environmental temperature.

The dependence of unfolding and refolding rate constants on denaturant concentration was analyzed according to the following linear relationship:[29,30]

$$\ln(k_{obs}) = \ln\{k_{UN}(H_2O)\exp[-(m_{UN}/RT)[GdmCl]] + k_{NU}(H_2O)\exp[(m_{NU}/RT)[GdmCl]]\} \quad (3)$$

where k_{obs} is the relaxation rate of unfolding or refolding measured at various GdmCl concentrations, $k_{UN}(H_2O)$ and $k_{NU}(H_2O)$ are the microscopic folding and unfolding rates, respectively, in the absence of denaturant, and m_{UN}/RT and m_{NU}/RT are proportionality constants, which describe the denaturant dependence. Bio-Kine 32 version 4.51 was used for nonlinear least-squares analysis of the data.

RESULTS AND DISCUSSION

Production of Trigger Factors. The genes encoding the TFs were cloned from the genomic DNA of *P. haloplanktis*, *E. coli*, and *T. maritima* on the basis of the known genome sequences. These genes were expressed in *E. coli* grown at 18 °C and purified to homogeneity. N-Terminal amino acid sequencing confirmed the identity of the proteins and indicated the persistence of the N-terminal formylmethionine. ESI-Q-TOF mass spectrometry also confirmed the expected mass of the proteins, as well as the absence of post-translational modifications. General data on the TFs are provided in Table 1. A preliminary characterization of *Ph*TF has previously been reported.[19]

Microcalorimetric Analysis of Stability. The thermal stability of the three TFs was investigated by DSC. Representative normalized thermograms are shown in Figure 1, and the corresponding microcalorimetric parameters are listed in Table 2. Figure 1 illustrates the drastic differences in the melting point, T_m (top of the transition), which varies from values as low as 33 °C for *Ph*TF to nearly the boiling point of water for *Tm*TF. This is accompanied by large increases in the microcalorimetric enthalpy, ΔH_{cal} (area under the transition). The latter parameter corresponds to the total amount of heat absorbed during unfolding, which is required to disrupt all enthalpy-driven interactions stabilizing the native state. Accordingly, both the T_m and ΔH_{cal} values depict the progressive enthalpic stabilization of the three TFs in parallel with the environmental temperature.

Although TF is a large multidomain protein, *Ph*TF unfolds cooperatively according to a two-state model, as indicated by a $\Delta H_{cal}/\Delta H_{vH}$ ratio close to unity (ΔH_{vH} is the van't Hoff enthalpy calculated from the slope of the normalized thermogram). The thermogram of *Ec*TF is asymmetric, however, and can be deconvoluted into two transitions (Figure 1) corresponding to two stability domains. Unfolding of the first one approximates a two-state process (Table 2), whereas the second transition deviates from such a model. Finally, the thermogram of *Tm*TF is symmetric, but the $\Delta H_{cal}/\Delta H_{vH}$ ratio above unity suggests the occurrence of two strongly interacting domains. We can conclude that the psychrophilic TF is uniformly unstable and unfolds cooperatively, whereas *Ec*TF and *Tm*TF contain two stability domains that perform improved interactions as the stability increases.

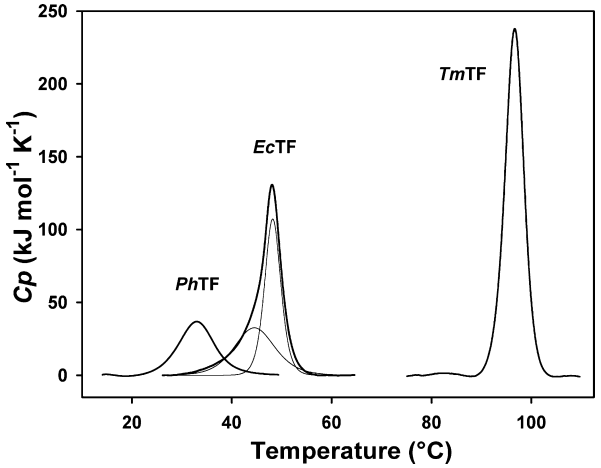

Figure 1. Differential scanning calorimetry of trigger factors. Analysis of the psychrophilic (*Ph*TF), mesophilic (*Ec*TF), and thermophilic (*Tm*TF) trigger factors in 30 mM Mops and 250 mM NaCl (pH 7.6). Baseline-subtracted thermograms have been normalized for protein concentration. For *Ec*TF, thin lines represent deconvolution of the thermogram into two cooperative transitions.

The psychrophilic TF displays an unusually high reversibility: 10 cycles of unfolding and refolding can be performed without a measurable loss of ΔH_{cal}. In addition, refolding upon cooling of the heat-denatured state can be recorded without compromising reversibility (Figure S1 of the Supporting Information). The high reversibility of another psychrophilic protein has been related to the low temperature of unfolding at which aggregation is not promoted.[15] However, *Ph*TF can be heated up to 90 °C without altering its unfolding reversibility. Accordingly, unfolding reversibility appears to be an intrinsic property of cold-adapted polypeptides. Unfolding of *Ec*TF under microcalorimetric conditions is accompanied by an ~10% loss of reversibility. This does not, however, preclude a thermodynamic analysis of the data as aggregation is slower than unfolding.[31] By contrast, in the presence of a nondetergent sulfobetaine, which prevents aggregation at the upper temperatures, unfolding of *Tm*TF is almost fully reversible. Finally, it is also worth mentioning that *Ph*TF is the least stable protein reported so far: at a mesophilic temperature of 37 °C, >90% of the protein molecules are already unfolded.

Change in Heat Capacity upon Unfolding. The heat capacity increment between the native and denatured states, ΔC_p, determines the temperature dependence of the Gibbs free energy of unfolding and hence the curvature of the stability plots (see below). The ΔC_p values recorded from the partial molar heat capacity of individual thermograms are listed in Table 2. In the case of the psychrophilic TF, which unfolds reversibly according to a two-state model, the ΔC_p value was also obtained experimentally using Kirchhoff's relation:

dx.doi.org/10.1021/bi4002387 | *Biochemistry* 2013, 52, 2982–2990

Table 2. Thermodynamic Parameters of Heat-Induced Unfolding Derived from Microcalorimetric Analysis of the Trigger Factors

trigger factor	T_m (°C)	ΔH_{cal} (kJ mol^{-1})	ΔH_{eff} (kJ mol^{-1})	$\Delta H_{cal}/\Delta H_{eff}$	reversibility (%)	ΔC_p (kJ mol^{-1} K^{-1})
*Ph*TF	33.0	345	330	1.04	>99	19.6
*Ec*TF	48.5	774			~90	19.6
first transition	44.6	333	311	1.07		
second transition	48.2	437	799	0.57		
*Tm*TF	96.6	1192	899	1.32	~98	11.3

$$\Delta C_p = \delta H/\delta T \quad (4)$$

Thermograms of *Ph*TF were recorded at decreasing pH values to destabilize the protein: a plot of ΔH_{cal} versus T_m yields a slope corresponding to a ΔC_p of 18.4 ± 1.4 kJ mol^{-1} K^{-1} (Figure S2 of the Supporting Information). Although obtained in a narrow range of stability, the latter value is in close agreement with data from individual thermograms. Such an experimental approach was not possible for *Ec*TF and *Tm*TF because of the heat-induced aggregation at pH values below neutrality.

Furthermore, the stability curve of the psychrophilic TF at low pH, computed with the corresponding ΔH_{cal}, T_m, and ΔC_p values, predicts a T_m for cold-unfolding near 0 °C (Figure S3 of the Supporting Information). As freezing of the protein solution can irremediably damage a microcalorimetric cell, the possible cold-unfolding of *Ph*TF was investigated by intrinsic fluorescence measurements. At pH 5.6, *Ph*TF undergoes heat-induced unfolding (Figure 2) with a T_m value of 28 °C, in accordance with DSC experiments (Figure 2, inset). Furthermore, when the sample is cooled to −4.1 °C, a clear cold-induced transition is also observed before freezing occurs, with a midpoint around 0 °C. This transition is reversible, and Figure 2 actually shows refolding of cold-denatured *Ph*TF, followed by unfolding at higher temperatures. It is worth mentioning that this is one of the very few reported cases in which the thermodynamic parameters derived from DSC experiments can be validated by determining experimentally the predicted cold-unfolding temperature.[32−34]

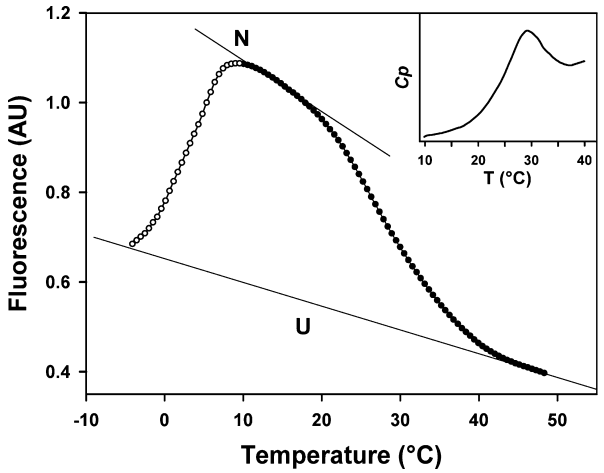

Figure 2. Cold-induced and heat-induced transitions of the psychrophilic TF monitored by fluorescence. The protein in 30 mM MES and 50 mM NaCl (pH 5.6) was cold-unfolded by being cooled to −4.1 °C (data points omitted for the sake of clarity) and then heated at a rate of 0.5 °C/min. Data for cold-refolding are shown with empty symbols. The refolded native state further undergoes heat-induced unfolding with a midpoint at 28 °C. Thin lines simulate the temperature dependence of fluorescence intensity of the native (N) and unfolded (U) states. Extrapolation of the latter suggests that cold-unfolding has nearly reached completion before freezing. The inset shows the raw microcalorimetric record of heat-induced unfolding under identical buffer conditions.

The ΔC_p value of the thermophilic TF may appear very low, as already noted for some heat-stable proteins.[32,35−37] This characteristic is rarely mentioned, but it has been shown that the difference in heat capacity between the native and unfolded states decreases with temperature and vanishes at around 120 °C for most mesophilic proteins.[38] It follows that the higher the melting temperature (as for *Tm*TF), the lower the ΔC_p value. This essential physicochemical property of the native and unfolded states should be taken into account in the analysis of the unusual stability of these proteins as it affects the shape of the stability curves (see below). In some cases, the occurrence of residual structures in the unfolded state of thermophilic proteins has been related to the low ΔC_p value.[36,37] To address this aspect, the three unfolded TFs were loaded via analytical (fast performance liquid chromatography) size exclusion chromatography in 4 M guanidinium chloride (GdmCl). The elution volume (and hence the hydrodynamic radius) was proportional to the number of amino acid residues in the sequence. Therefore, this technique does not provide evidence of substantial residual structures, i.e., reduction of the hydrodynamic radius, in the unfolded state of *Tm*TF.

Equilibrium Unfolding. GdmCl-induced unfolding of the three TFs was followed at 25 °C by measuring the intrinsic fluorescence emission. Data collected at two different wavelengths, i.e., 307 and 335 nm for tyrosine and tryptophan residues, respectively, provided identical results. Figure 3 illustrates the reversible unfolding transitions obtained under equilibrium conditions, and the corresponding thermodynamic parameters are listed in Table 3. The conformational stability of these proteins [given by the Gibbs free energy of unfolding, $\Delta G°(H_2O)_{NU}$] increases in parallel with both their thermal stability and their environmental temperatures. *Ph*TF unfolds cooperatively according to a two-state transition and is only marginally stable (5 kJ/mol). By contrast, the unfolding curves of both *Ec*TF and *Tm*TF are best fit using a three-state unfolding mechanism. Two discrete transitions are readily observed for *Ec*TF (Figure 3), as previously reported,[39] and a three-state model is required to analyze experimental data for *Tm*TF. For both proteins, chemical unfolding is not fully cooperative, in good agreement with DSC results. Data in Figure 3 allowed delineation of the experimental conditions for the kinetic experiments described below.

Folding and Unfolding Kinetics. To address the kinetic origin of the large differences in stability observed for TFs, both folding and unfolding kinetics were followed by stopped-flow fluorescence spectroscopy. Because the equilibrium constant K_{NU} between the native state N and the unfolding state U is equal to the ratio k_{NU}/k_{UN} of the kinetic constants for unfolding

dx.doi.org/10.1021/bi4002387 | *Biochemistry* 2013, 52, 2982−2990

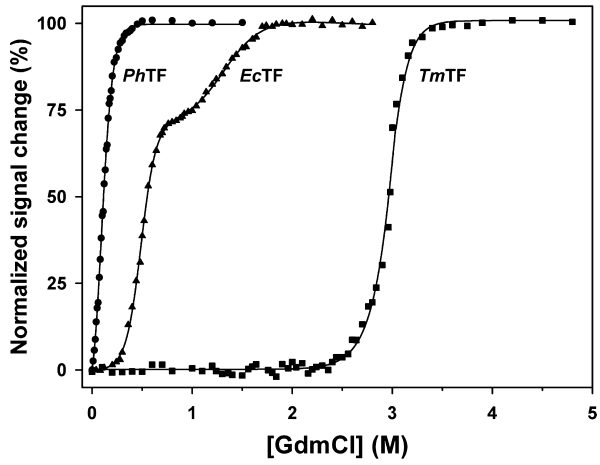

Figure 3. GdmCl-induced equilibrium unfolding of trigger factors: *Ph*TF (●), *Ec*TF (▲), and *Tm*TF (■). The normalized fluorescence signal changes (pre- and post-transition baselines subtracted) for unfolding are shown as a function of GdmCl concentration. Solid lines represent least-squares fit analyses of the experimental data according to a two-state (*Ph*TF) or three-state (*Ec*TF and *Tm*TF) unfolding mechanism.

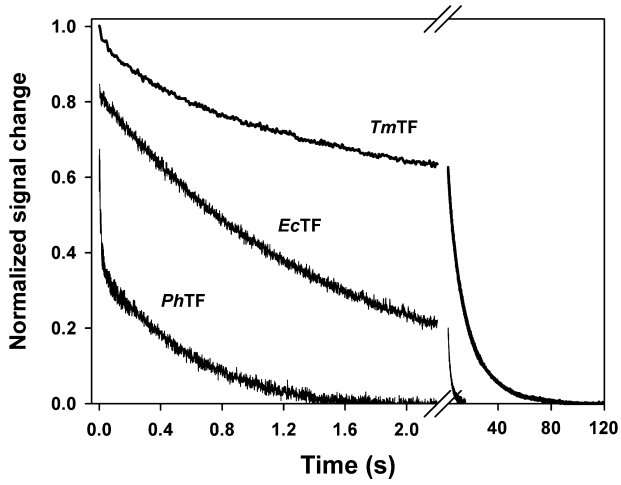

Figure 4. Kinetics of unfolding monitored by stopped-flow fluorescence. Records for *Ph*TF and *Ec*TF, both in 1 M GdmCl, and for *Tm*TF in 3 M GdmCl. Kinetic traces are normalized for identical initial (fluorescence intensity of the initial state, mixed with buffer without GdmCl) and final (steady-state fluorescence intensity) values.

and folding, an increase in protein stability can be achieved either by slower unfolding (k_{NU}) or by faster refolding (k_{UN}), or possibly by a combination of both.

Unfolding of the three TFs was induced by fast 10-fold dilution of the native proteins at various GdmCl concentrations. Typical unfolding kinetic records are shown in Figure 4. In the presence of 1 M GdmCl, the marginally stable *Ph*TF is completely unfolded in <2 s, unfolding of *Ec*TF is 10 times slower under the same conditions, and *Tm*TF unfolds 50 times slower in 3 M GdmCl. The observed kinetics were analyzed as the sum of three or four (*Tm*TF) exponential functions, and the corresponding rate constant values form the right branch of the chevron plots shown in Figure 5. In refolding experiments, TFs were first fully unfolded after incubation for 24 h in concentrated GdmCl, and then refolding was initiated by fast dilution to various final GdmCl concentrations. The observed refolding kinetic traces are described well by the sum of two or three (*Tm*TF) exponential functions, and the corresponding rate constant values form the left branch of the chevron plots in Figure 5. Such complex folding and unfolding kinetics probably reflect the three-domain structural organization of TFs.

These chevron plots allow the determination of the microscopic folding and unfolding rate constants in the absence of denaturant, $k_{NU}(H_2O)$ and $k_{UN}(H_2O)$, by linear regression on the ordinate (dashed lines in Figure 5, Table 4, and Table S1 of the Supporting Information). These extrapolations are enlarged in Figure 6. Despite the complexity of TF folding and unfolding kinetics, a clear trend is observed: the large differences in stability among the three TFs are mainly due to the large differences in the unfolding rates. Both the slow and fast folding phases are clustered in a narrow range of $k_{UN}(H_2O)$ values that differ by only 1 or 2 orders of magnitude (Figure 6 and Table 4). In sharp contrast, the unfolding rate constants, $k_{NU}(H_2O)$, differ by 8 orders of magnitude between *Ph*TF and *Tm*TF. Furthermore, *Tm*TF displays an additional very slow unfolding phase when compared with both homologues. In this respect, the slow unfolding to achieve high stability previously reported for hyperthermophilic proteins[13,40,41] is also observed for *Tm*TF. More importantly, fast unfolding is the main determinant of *Ph*TF's low stability, while *Ec*TF displays intermediate values. There is, therefore, a continuum in the resistance to unfolding that kinetically drives adjustments of stability at environmental temperatures. This also suggests that the free energy level of the transition state in the unfolding pathway modulates the stability of proteins over the whole range of biological temperatures. Folding and unfolding kinetics were also recorded at 9 °C by manual mixing, yielding qualitatively similar results for the observable phases (Figure S4 of the Supporting Information). It is also worth mentioning that stabilized, mesophilic-like mutants of a psychrophilic α-amylase display similar properties[42] (i.e., identical folding rates but slower unfolding rates with respect to that of the native heat-labile protein), suggesting convergence of kinetic contributions to stability in cold-adapted proteins.

Stability Curves and Thermodynamic Stability. The stability curves of the three TFs have been computed in Figure

Table 3. Thermodynamic Parameters of Equilibrium Unfolding in GdmCl for Trigger Factors at 25 °C

	trigger factor	$-m_i$ (kJ mol^{-1} M^{-1})	$\Delta G°(H_2O)_i$ (kJ mol^{-1})	C_m (M)	$-m_{NU}$ (kJ mol^{-1} M^{-1})	$\Delta G°(H_2O)_{NU}$ (kJ mol^{-1})
*Ph*TF				0.10 ± 0.007	51.2 ± 1.8	5.2 ± 0.3
*Ec*TF						
	first transition	33.3 ± 1.4	16.2 ± 0.8	0.49 ± 0.03	46.6 ± 2.9	33.9 ± 2.3
	second transition	13.3 ± 1.2	17.7 ± 1.5	1.33 ± 0.16		
*Tm*TF						
	first transition	14.9 ± 7.9	41.6 ± 8.8	2.79 ± 1.5	54.7 ± 13.5	160.4 ± 17.4
	second transition	39.8 ± 5.6	118.8 ± 8.6	2.98 ± 0.5		

dx.doi.org/10.1021/bi4002387 | *Biochemistry* 2013, 52, 2982−2990

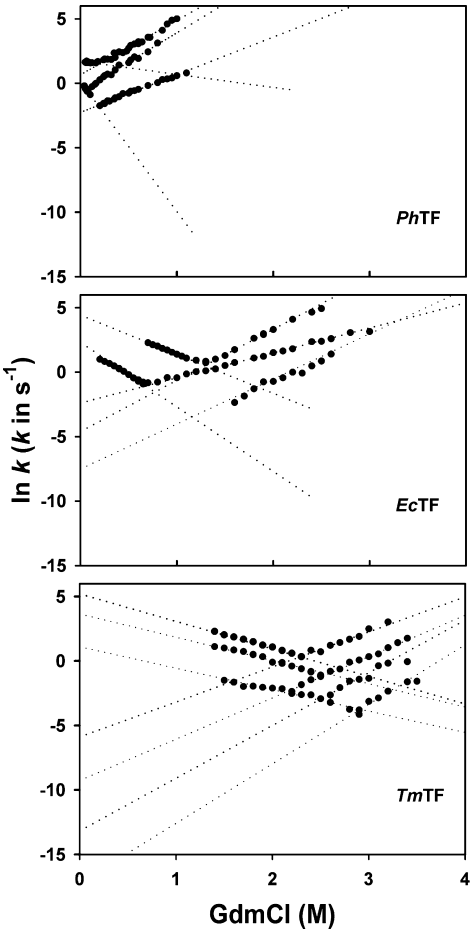

Figure 5. Folding and unfolding kinetics quantified by stopped-flow fluorescence spectroscopy. Chevron plots of the GdmCl concentration dependence of the relaxation rate constants for unfolding (right arms of the plot) and refolding (left arms) at 20 °C. Data are shown for *Ph*TF, *Ec*TF, and *Tm*TF. Dashed lines are extrapolations to 0 M GdmCl allowing the determination of $k_{NU}(H_2O)$ and $k_{UN}(H_2O)$, the microscopic unfolding and folding rate constants, respectively, in the absence of a denaturant.

Table 4. Microscopic Folding and Unfolding Rate Constants at 20 °C for TFs Determined by Stopped-Flow Fluorescence Spectroscopy

	rate constant (s^{-1})			
trigger factor	phase 1	phase 2	phase 3	phase 4
	Folding, $k_{UN}(H_2O)$			
*Ph*TF	–[a]	5.4	1.1	
*Ec*TF	–[a]	82.3	9.9	
*Tm*TF	182.5	37.9	3.0	
	Unfolding, $k_{NU}(H_2O)$			
*Ph*TF	1.9	0.5	0.1	
*Ec*TF	9.1×10^{-2}	9.9×10^{-3}	5.4×10^{-4}	
*Tm*TF	2.7×10^{-3}	9.3×10^{-5}	1.9×10^{-6}	3.3×10^{-8}

[a]Not observed.

7 using the microcalorimetric parameters (Table 2) and the modified Gibbs–Helmholtz relation:

$$\Delta G_{NU}(T) = \Delta H_{cal}(1 - T/T_m) + \Delta C_p(T - T_m) - T\Delta C_p \ln(T/T_m) \quad (5)$$

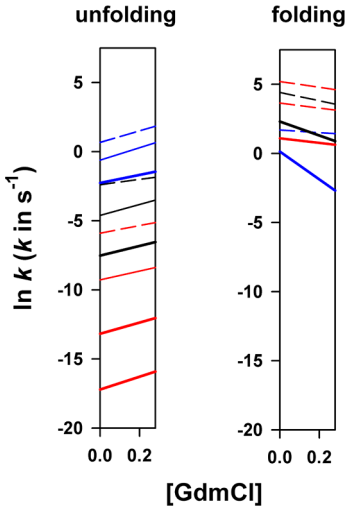

Figure 6. Close-up of ordinate extrapolations. Extrapolations of the relaxation rate constants for the determination of microscopic unfolding and folding rate constants in the absence of denaturant. Data are shown for *Ph*TF (blue lines), *Ec*TF (black lines), and *Tm*TF (red lines). Fast (dashed lines), medium (thin lines), and slow (thick lines) phases should be compared. Folding rate constants are clustered in a narrow range of $k_{UN}(H_2O)$ values, whereas unfolding rate constants, $k_{NU}(H_2O)$, differ by 8 orders of magnitude.

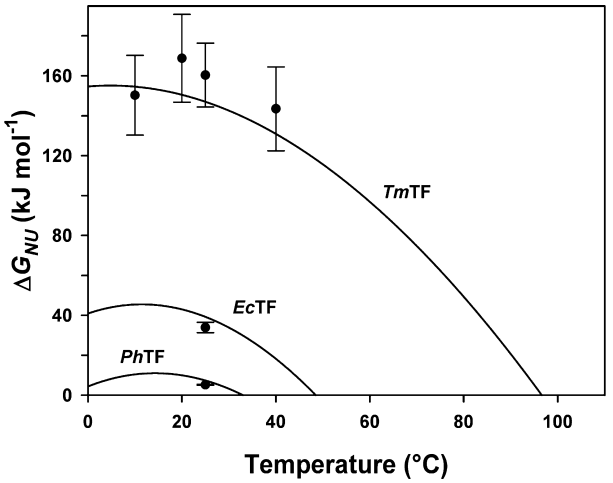

Figure 7. Stability curves of trigger factors. Curves computed from the Gibbs free energy of unfolding and microcalorimetric parameters for *Ph*TF, *Ec*TF, and *Tm*TF. Filled symbols correspond to individual $\Delta G°(H_2O)_{NU}$ values obtained from equilibrium unfolding in GdmCl at various temperatures.

This Gibbs free energy function corresponds to the work required to unfold the native state at any given temperature and, by definition, is zero at the melting point, T_m. The individual $\Delta G°(H_2O)_{NU}$ values obtained from equilibrium unfolding in GdmCl are also reported. A satisfactory agreement between both experimental approaches is observed, which allows us to draw some general conclusions.

(i) The high stability of the thermophilic TF is obtained by the uplift of its stability curve toward larger ΔG_{NU} values, whereas the weak stability of the psychrophilic TF corresponds to a global lowering of its free energy function, as compared with that of the mesophilic protein. This is the obvious consequence of drastic differences in enthalpic stabilization characterized by the T_m and ΔH_{cal} values listed in Table 2. This

dx.doi.org/10.1021/bi4002387 | *Biochemistry* 2013, 52, 2982–2990

also indicates that enthalpy-driven interactions play a prominent role in the adjustments of the conformational stability, as already suggested by three-dimensional structures of psychrophilic and hyperthermophilic proteins.[43−46]

(ii) The three curves in Figure 7 display roughly similar shapes in the temperature range considered. In the case of *Tm*TF, the similar plot curvature arises from the low ΔC_p associated with high ΔH_{cal} values. Indeed, a simulation using a ΔC_p value of 19.6 kJ mol^{-1} K^{-1} (as for *Ec*TF) yields a much sharper stability curve, incompatible with the experimental $\Delta G^{\circ}(H_2O)_{NU}$ values. Accordingly, there is a fine-tuning of thermodynamic parameters ΔH_{cal}, ΔC_p, and T_m in proteins adapted to extreme temperatures, leading to the similar shapes of their free energy functions.

(iii) There is no significant displacement of the maximal stability (top of the bell-shaped curves in Figure 7), neither toward high temperatures for the thermophilic TF nor toward low temperatures for the psychrophilic TF: maximal stability is reached near room temperature, irrespective of the thermal regime of the source microorganism. A similar conclusion was previously reached by comparing proteins with distinct stabilities,[47−49] and it appears that this conclusion can be extended to extremophilic proteins, as far as TFs are concerned. It has been suggested that a common temperature for maximal stability arises from an optimal hydrophobic effect in this temperature range[48] or, more generally, from the balance between enthalpic interactions and hydration effects on the various protein groups.[50]

(iv) A surprising consequence of the collapsed free energy function of the psychrophilic TF is its weak stability at low temperatures: *Ph*TF is, in fact, both heat- and cold-labile in vitro. Cold-adapted polypeptides are therefore prone to cold-unfolding, and this can be an additional factor limiting life at low temperatures. It is worth mentioning that polar bacteria such a *P. haloplanktis* become trapped in the winter ice pack and experience long-term freezing.[7] It can be suggested here that the unusual unfolding reversibility noted for psychrophilic proteins is an adaptive trait aimed at recovering functional proteins upon thawing if cold-unfolding has occurred.

(v) The stability curves in Figure 7 should also be analyzed with respect to environmental temperatures. These temperatures for *Ec*TF and *Tm*TF fall on the right limb of the bell-shaped curves, and therefore, the thermal dissipative forces (leading to thermal denaturation) promote molecular motions required for proper protein function. By contrast, environmental temperatures for the psychrophilic TF lie on the left limb of its stability curve. As a consequence, molecular motions at low temperatures are promoted by factors that ultimately lead to cold-unfolding. Hydration of polar and nonpolar groups at low temperatures is currently regarded as the driving force of cold-unfolding[50] and should be involved in the dynamics of the psychrophilic TF in the cold.

(vi) Finally, at temperatures above the maximal stability, the enthalpic contribution is a stabilizing factor. However, at temperatures below the maximal stability, both the enthalpic and entropic terms change their sign and the enthalpic contribution becomes a destabilizing factor.[51] It follows that at environmental temperatures, the stability of *Ph*TF is entropy-driven, in sharp contrast with those of its mesophilic and hyperthermophilic homologues.

Interestingly, the analysis of the *Ph*TF stability curve is in agreement with earlier data on a psychrophilic α-amylase,[15] indicating common traits in cold-adapted proteins.

CONCLUSIONS

We have shown here that adjustments of protein stability over the whole range of biological temperatures proceed via the same fundamental mechanisms. This involves increases in the level of enthalpic stabilization and in resistance to unfolding with increased environmental temperatures. These results provide evidence that neither the unusually stable hyperthermophilic proteins nor the natively unstable psychrophilic proteins have evolved specific mechanisms for reaching the necessary balance between stability and dynamics,[52,53] ensuring functionality at their respective environmental temperatures. Rather, their thermodynamic and kinetic stability parameters are part of a continuum ranging from low to moderate and high temperatures. The striking parallel between enthalpic stabilization noted here and the number of weak interactions and of stabilization factors observed in the three-dimensional structures of psychrophilic, mesophilic, and hyperthermophilic proteins provides a sound basis for explaining the differences in thermal stability. By contrast, the next challenge will be to characterize the energetics of the transition-state intermediate on the unfolding pathway that modulates the kinetic stability of these proteins. Obviously, small model proteins are required to reach this goal.

ASSOCIATED CONTENT

Supporting Information

Figures S1−S3 and Table S1. This material is available free of charge via the Internet at http://pubs.acs.org.

AUTHOR INFORMATION

Corresponding Author

*Laboratory of Biochemistry, Center for Protein Engineering, Institute of Chemistry B6a, B-4000 Liège-Sart Tilman, Belgium. Telephone: +32 4 366 33 43. Fax: +32 4 366 33 64. E-mail: gfeller@ulg.ac.b.

Funding

This work was supported by the FRS-FNRS, Belgium (Fonds de la Recherche Fondamentale et Collective, Contracts 2.4535.08 to G.F. and 2.4530.09 to A.M.), and by the Belgian program of Interuniversity Attraction Poles (iPros P7/44) initiated by the Federal Office for Scientific, Technical and Cultural Affaires. C.S. is a FRS-FNRS research fellow.

Notes

The authors declare no competing financial interest.

ACKNOWLEDGMENTS

We thank R. Barumandzadeh for expert assistance in stopped-flow experiments.

ABBREVIATIONS

*Ph*TF, *P. haloplanktis* trigger factor; *Ec*TF, *E. coli* trigger factor; *Tm*TF, *T. maritima* trigger factor; GdmCl, guanidine hydrochloride.

REFERENCES

(1) Gerday, C., and Glansdorff, N. (2007) *Physiology and Biochemistry of Extremophiles*, ASM Press, Washington, DC.

(2) Horikoshi, K., Antranikian, G., Bull, A. T., Robb, F. T., and Stetter, K. O., Eds. (2011) *Extremophiles Handbook*, Springer-Verlag, Tokyo.

(3) Takai, K., Nakamura, K., Toki, T., Tsunogai, U., Miyazaki, M., Miyazaki, J., Hirayama, H., Nakagawa, S., Nunoura, T., and Horikoshi,

K. (2008) Cell proliferation at 122 °C and isotopically heavy CH_4 production by a hyperthermophilic methanogen under high-pressure cultivation. *Proc. Natl. Acad. Sci. U.S.A. 105*, 10949−10954.
(4) Feller, G., and Gerday, C. (2003) Psychrophilic enzymes: Hot topics in cold adaptation. *Nat. Rev. Microbiol. 1*, 200−208.
(5) Margesin, R., Schinner, F., Marx, J. C., and Gerday, C. (2008) *Psychrophiles, from Biodiversity to Biotechnology*, Springer-Verlag, Berlin.
(6) Rodrigues, D. F., and Tiedje, J. M. (2008) Coping with our cold planet. *Appl. Environ. Microbiol. 74*, 1677−1686.
(7) Deming, J. W. (2002) Psychrophiles and polar regions. *Curr. Opin. Microbiol. 5*, 301−309.
(8) Siddiqui, K. S., and Cavicchioli, R. (2006) Cold-adapted enzymes. *Annu. Rev. Biochem. 75*, 403−433.
(9) Smalas, A. O., Leiros, H. K., Os, V., and Willassen, N. P. (2000) Cold adapted enzymes. *Biotechnol. Annu. Rev. 6*, 1−57.
(10) Karshikoff, A., and Ladenstein, R. (2001) Ion pairs and the thermotolerance of proteins from hyperthermophiles: A "traffic rule" for hot roads. *Trends Biochem. Sci. 26*, 550−556.
(11) Szilagyi, A., and Zavodszky, P. (2000) Structural differences between mesophilic, moderately thermophilic and extremely thermophilic protein subunits: Results of a comprehensive survey. *Structure 8*, 493−504.
(12) Vieille, C., and Zeikus, G. J. (2001) Hyperthermophilic enzymes: Sources, uses, and molecular mechanisms for thermostability. *Microbiol. Mol. Biol. Rev. 65*, 1−43.
(13) Luke, K. A., Higgins, C. L., and Wittung-Stafshede, P. (2007) Thermodynamic stability and folding of proteins from hyperthermophilic organisms. *FEBS J. 274*, 4023−4033.
(14) Mukaiyama, A., and Takano, K. (2009) Slow unfolding of monomeric proteins from hyperthermophiles with reversible unfolding. *Int. J. Mol. Sci. 10*, 1369−1385.
(15) Feller, G., d'Amico, D., and Gerday, C. (1999) Thermodynamic stability of a cold-active α-amylase from the Antarctic bacterium *Alteromonas haloplanctis*. *Biochemistry 38*, 4613−4619.
(16) Hartl, F. U., and Hayer-Hartl, M. (2009) Converging concepts of protein folding *in vitro* and *in vivo*. *Nat. Struct. Mol. Biol. 16*, 574−581.
(17) Martinez-Hackert, E., and Hendrickson, W. A. (2009) Promiscuous substrate recognition in folding and assembly activities of the trigger factor chaperone. *Cell 138*, 923−934.
(18) Merz, F., Boehringer, D., Schaffitzel, C., Preissler, S., Hoffmann, A., Maier, T., Rutkowska, A., Lozza, J., Ban, N., Bukau, B., and Deuerling, E. (2008) Molecular mechanism and structure of Trigger Factor bound to the translating ribosome. *EMBO J. 27*, 1622−1632.
(19) Piette, F., D'Amico, S., Struvay, C., Mazzucchelli, G., Renaut, J., Tutino, M. L., Danchin, A., Leprince, P., and Feller, G. (2010) Proteomics of life at low temperatures: Trigger factor is the primary chaperone in the Antarctic bacterium *Pseudoalteromonas haloplanktis* TAC125. *Mol. Microbiol. 76*, 120−132.
(20) D'Amico, S., and Feller, G. (2009) A nondetergent sulfobetaine improves protein unfolding reversibility in microcalorimetric studies. *Anal. Biochem. 385*, 389−391.
(21) Nozaki, Y. (1972) The preparation of guanidine hydrochloride. *Methods Enzymol. 26*, 43−50.
(22) Santoro, M. M., and Bolen, D. W. (1988) Unfolding free energy changes determined by the linear extrapolation method. 1. Unfolding of phenylmethanesulfonyl α-chymotrypsin using different denaturants. *Biochemistry 27*, 8063−8068.
(23) Pace, C. N. (1990) Measuring and increasing protein stability. *Trends Biotechnol. 8*, 93−98.
(24) Vandenameele, J., Lejeune, A., Di Paolo, A., Brans, A., Frere, J. M., Schmid, F. X., and Matagne, A. (2010) Folding of class A β-lactamases is rate-limited by peptide bond isomerization and occurs via parallel pathways. *Biochemistry 49*, 4264−4275.
(25) Barrick, D., and Baldwin, R. L. (1993) Three-state analysis of sperm whale apomyoglobin folding. *Biochemistry 32*, 3790−3796.
(26) Matthews, C. R., and Crisanti, M. M. (1981) Urea-induced unfolding of the α subunit of tryptophan synthase: Evidence for a multistate process. *Biochemistry 20*, 784−792.
(27) Nishikori, S., Shiraki, K., Fujiwara, S., Imanaka, T., and Takagi, M. (2005) Unfolding mechanism of a hyperthermophilic protein O(6)-methylguanine-DNA methyltransferase. *Biophys. Chem. 116*, 97−104.
(28) Soulages, J. L. (1998) Chemical denaturation: Potential impact of undetected intermediates in the free energy of unfolding and m-values obtained from a two-state assumption. *Biophys. J. 75*, 484−492.
(29) Fersht, A. R. (1999) *Structure and Mechanism in Protein Science: A Guide to Enzyme Catalysis and Protein Folding*, W. H. Freeman and Co., New York.
(30) Khorasanizadeh, S., Peters, I. D., and Roder, H. (1996) Evidence for a three-state model of protein folding from kinetic analysis of ubiquitin variants with altered core residues. *Nat. Struct. Biol. 3*, 193−205.
(31) Privalov, G. P., and Privalov, P. L. (2000) Problems and prospects in microcalorimetry of biological macromolecules. *Methods Enzymol. 323*, 31−62.
(32) Knapp, S., Karshikoff, A., Berndt, K. D., Christova, P., Atanasov, B., and Ladenstein, R. (1996) Thermal unfolding of the DNA-binding protein Sso7d from the hyperthermophile *Sulfolobus solfataricus*. *J. Mol. Biol. 264*, 1132−1144.
(33) Novokhatny, V., and Ingham, K. (1997) Thermodynamics of maltose binding protein unfolding. *Protein Sci. 6*, 141−146.
(34) Privalov, P. L. (1990) Cold denaturation of proteins. *Crit. Rev. Biochem. Mol. Biol. 25*, 281−305.
(35) McCrary, B. S., Edmondson, S. P., and Shriver, J. W. (1996) Hyperthermophile protein folding thermodynamics: Differential scanning calorimetry and chemical denaturation of Sac7d. *J. Mol. Biol. 264*, 784−805.
(36) Robic, S., Guzman-Casado, M., Sanchez-Ruiz, J. M., and Marqusee, S. (2003) Role of residual structure in the unfolded state of a thermophilic protein. *Proc. Natl. Acad. Sci. U.S.A. 100*, 11345−11349.
(37) Wallgren, M., Aden, J., Pylypenko, O., Mikaelsson, T., Johansson, L. B., Rak, A., and Wolf-Watz, M. (2008) Extreme temperature tolerance of a hyperthermophilic protein coupled to residual structure in the unfolded state. *J. Mol. Biol. 379*, 845−858.
(38) Privalov, P. L., and Dragan, A. I. (2007) Microcalorimetry of biological macromolecules. *Biophys. Chem. 126*, 16−24.
(39) Liu, C. P., Li, Z. Y., Huang, G. C., Perrett, S., and Zhou, J. M. (2005) Two distinct intermediates of trigger factor are populated during guanidine denaturation. *Biochimie 87*, 1023−1031.
(40) Okada, J., Okamoto, T., Mukaiyama, A., Tadokoro, T., You, D. J., Chon, H., Koga, Y., Takano, K., and Kanaya, S. (2010) Evolution and thermodynamics of the slow unfolding of hyperstable monomeric proteins. *BMC Evol. Biol. 10*, 207.
(41) Perl, D., Welker, C., Schindler, T., Schroder, K., Marahiel, M. A., Jaenicke, R., and Schmid, F. X. (1998) Conservation of rapid two-state folding in mesophilic, thermophilic and hyperthermophilic cold shock proteins. *Nat. Struct. Biol. 5*, 229−235.
(42) Cipolla, A., D'Amico, S., Barumandzadeh, R., Matagne, A., and Feller, G. (2011) Stepwise adaptations to low temperature as revealed by multiple mutants of psychrophilic α-amylase from Antarctic bacterium. *J. Biol. Chem. 286*, 38348−38355.
(43) Bae, E., and Phillips, G. N., Jr. (2004) Structures and analysis of highly homologous psychrophilic, mesophilic, and thermophilic adenylate kinases. *J. Biol. Chem. 279*, 28202−28208.
(44) Bell, G. S., Russell, R. J., Connaris, H., Hough, D. W., Danson, M. J., and Taylor, G. L. (2002) Stepwise adaptations of citrate synthase to survival at life's extremes. From psychrophile to hyperthermophile. *Eur. J. Biochem. 269*, 6250−6260.
(45) Linden, A., and Wilmanns, M. (2004) Adaptation of class-13 α-amylases to diverse living conditions. *ChemBioChem 5*, 231−239.
(46) Zheng, B., Yang, W., Zhao, X., Wang, Y., Lou, Z., Rao, Z., and Feng, Y. (2012) Crystal structure of hyperthermophilic endo-β-1,4-glucanase: Implications for catalytic mechanism and thermostability. *J. Biol. Chem. 287*, 8336−8346.
(47) Kumar, S., and Nussinov, R. (2004) Experiment-guided thermodynamic simulations on reversible two-state proteins: Implications for protein thermostability. *Biophys. Chem. 111*, 235−246.

(48) Kumar, S., Tsai, C. J., and Nussinov, R. (2002) Maximal stabilities of reversible two-state proteins. *Biochemistry 41*, 5359−5374.
(49) Rees, D. C., and Robertson, A. D. (2001) Some thermodynamic implications for the thermostability of proteins. *Protein Sci. 10*, 1187−1194.
(50) Makhatadze, G. I., and Privalov, P. L. (1995) Energetics of protein structure. *Adv. Protein Chem. 47*, 307−425.
(51) Privalov, P. (1992) Physical basis of the stability of the folded conformations of proteins. In *Protein Folding* (Creighton, T., Ed.) pp 83−126, W. H. Freeman and Co., New York.
(52) Baldwin, A. J., and Kay, L. E. (2009) NMR spectroscopy brings invisible protein states into focus. *Nat. Chem. Biol. 5*, 808−814.
(53) Zavodszky, P., Kardos, J., Svingor, A., and Petsko, G. A. (1998) Adjustment of conformational flexibility is a key event in the thermal adaptation of proteins. *Proc. Natl. Acad. Sci. U.S.A. 95*, 7406−7411.

Supporting Information to:

Energetics of protein stability at extreme environmental temperatures in bacterial trigger factors

Caroline Struvay[†], Sonia Negro[†], André Matagne[‡] and Georges Feller[†]

[†] Laboratory of Biochemistry and [‡] Laboratory of Enzymology and Protein Folding, Center for Protein Engineering, University of Liège, B-4000 Liège-Sart Tilman, Belgium

Contents

The abbreviation used are: *Ph*TF, *Pseudoalteromonas haloplanktis* trigger factor; *Ec*TF, *Escherichia coli* trigger factor; *Tm*TF, *Thermotoga maritima* trigger factor; GdmCl, guanidine hydrochloride.

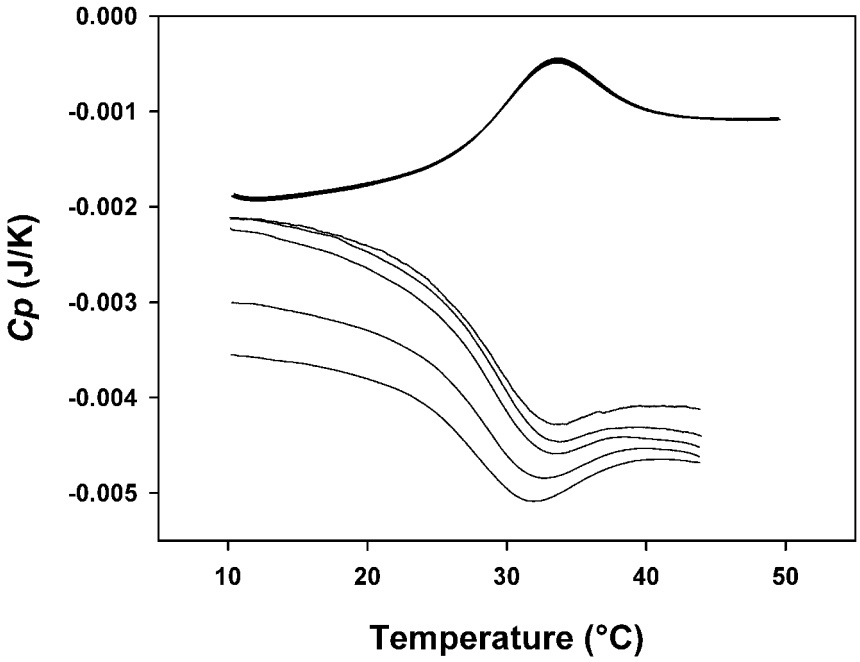

Fig. S1: Reversibility of heat-induced unfolding and refolding of the psychrophilic TF. Raw microcalorimetric data showing five consecutive scan cycles without refilling in 30 mM MOPS, 250 mM NaCl, pH 7.6. Up-scans (upper curves) were performed at 60 K h^{-1}: the excellent thermogram superimposition demonstrates full unfolding reversibility. Down-scans (lower curves) were performed at 90 (lower trace), 60, 30, 15 and 7.5 K h^{-1} (thermograms have been displaced along the ordinate for clarity).

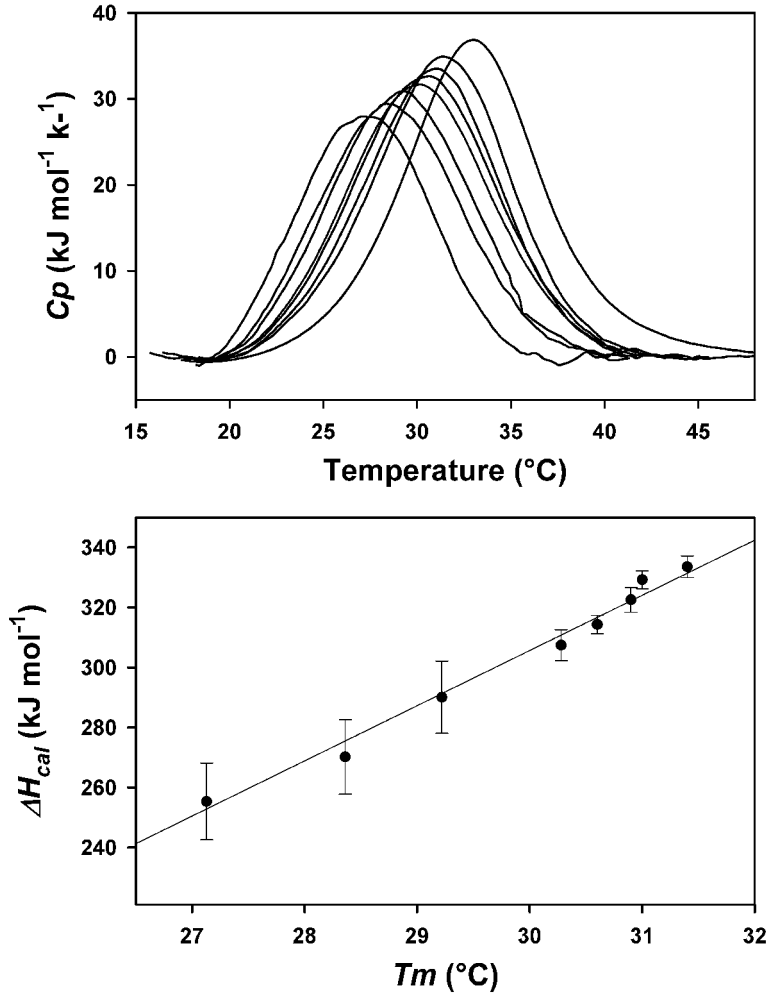

Fig. S2: Determination of the ΔCp value for the psychrophilic TF. Upper panel: normalized thermograms of *Ph*TF at decreasing pH (from right to left, pH 7.6, 6.7, 6.5, 6.3, 6.2, 6.1, 6.0 and 5.9) in 30 mM MES, 250 mM NaCl (30 mM MOPS at pH 7.6). Lower panel: plot of the microcalorimetric enthalpy, ΔH_{cal} versus the melting point, *Tm*. According to the Kirchhoff relation, $\Delta Cp = \delta H / \delta T$, the plot slope corresponds to $\Delta Cp = 18.4 \pm 1.4$ kJ mol^{-1} K^{-1}.

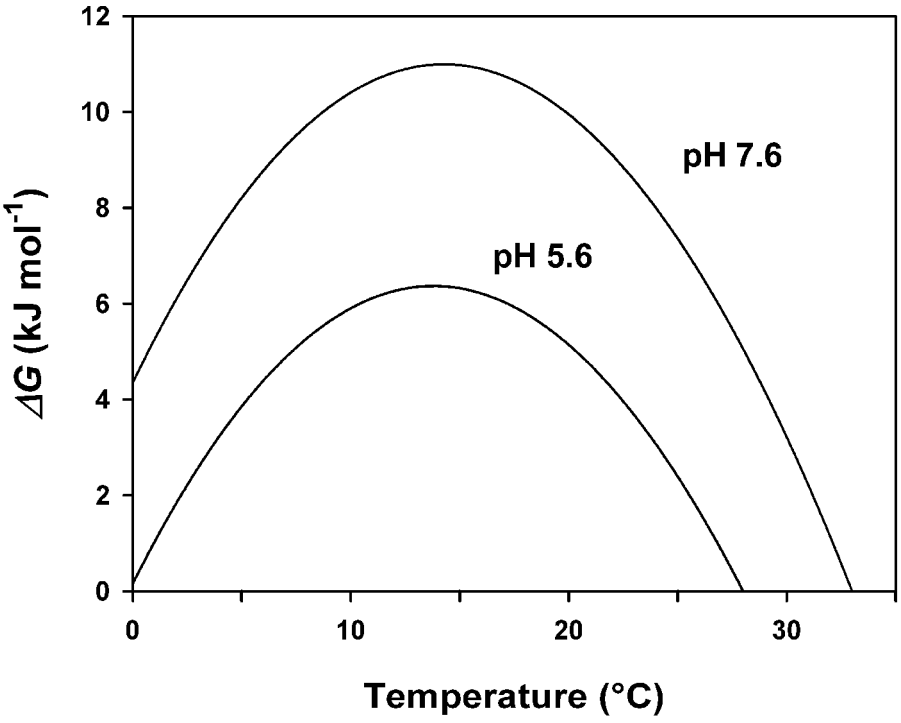

Fig. S3: Stability curves predict cold unfolding of *Ph*TF. Stability curves of the psychrophilic TF under physiological conditions and at low pH computed from the modified Gibbs-Helmholtz relation. Cold unfolding is predicted around 0°C at pH 5.6. The following values were used at pH 7.6: ΔH_{cal} = 345 kJ mol^{-1}, *Tm* = 33 °C and ΔCp = 18.4 kJ mol^{-1} K^{-1}; at pH 5.6: ΔH_{cal} = 268 kJ mol^{-1}, *Tm* = 28 °C as recorded by DSC in 30 mM MES, 50 mM NaCl.

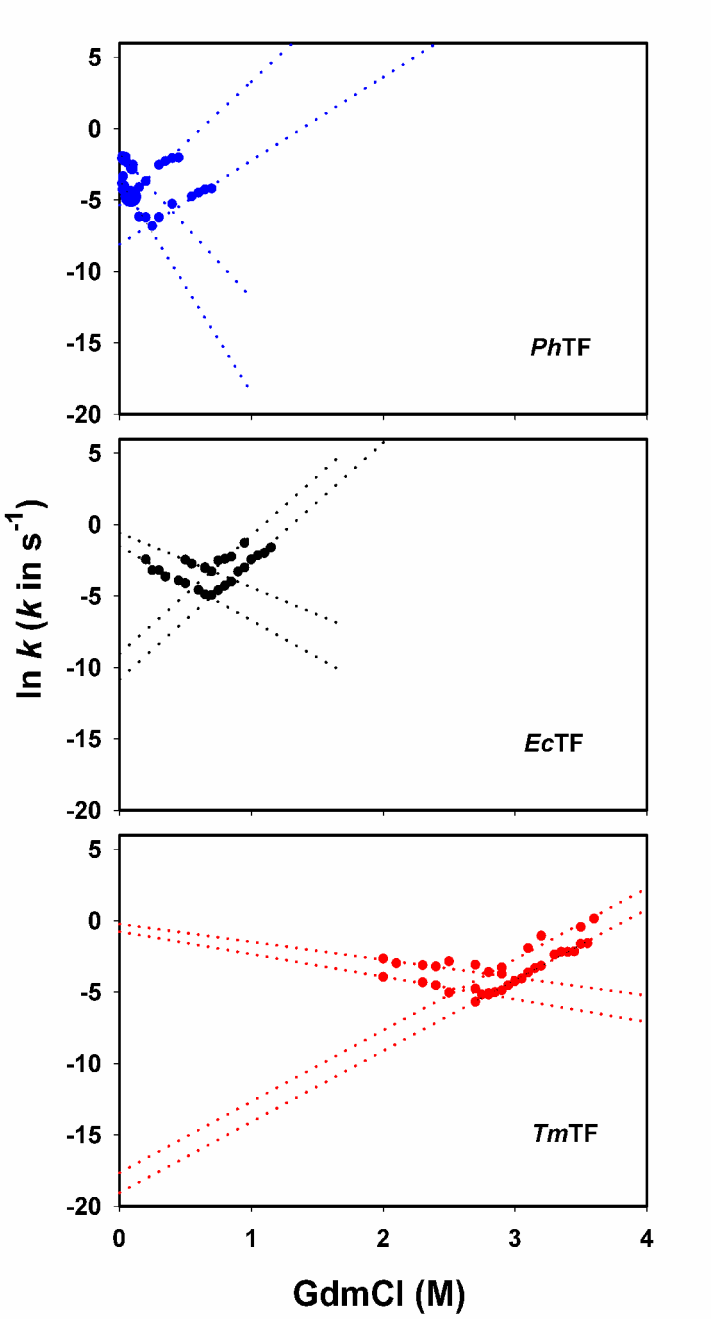

Fig. S4: Folding and unfolding kinetics at 9°C recorded by manual mixing fluorescence. Chevron plots of the GdmCl concentration dependence of the relaxation rate constants for unfolding (right arms of the plot) and refolding (left arms). Dashed lines are extrapolations to 0 M GdmCl.

Table S1

Microscopic rate constants and kinetic *m*-values of folding, ln($k_{UN}H_20$) and m_{UN}, and of unfolding, ln($k_{NU}H_20$) and m_{NU}, at 20°C determined from stopped-flow experiments

Trigger Factor		*Phase 1*	*Phase 2*	*Phase 3*	*Phase 4*
	Folding				
*Ph*TF	ln($k_{UN}H_20$)		1.69 ± 0.04	0.13 ± 0.07	
	m_{UN} (M^{-1})		-1.01 ± 0.59	-10.07 ± 1.12	
*Ec*TF	ln($k_{UN}H_20$)		4.41 ± 0.05	2.30 ± 0.04	
	m_{UN} (M^{-1})		-3.03 ± 0.06	-5.00 ± 0.07	
*Tm*TF	ln($k_{UN}H_20$)	5.21 ± 0.14	3.64 ± 0.12	1.10 ± 0.22	
	m_{UN} (M^{-1})	-2.13 ± 0.08	-1.80 ± 0.07	-1.66 ± 0.10	
	Unfolding				
*Ph*TF	ln($k_{NU}H_20$)	0.66 ± 0.09	-0.62 ± 0.10	-2.27 ± 0.03	
	m_{NU} (M^{-1})	4.21 ± 0.15	4.53 ± 0.23	2.92 ± 0.06	
*Ec*TF	ln($k_{NU}H_20$)	-2.40 ± 0.25	-4.61 ± 0.19	-7.53 ± 0.60	
	m_{NU} (M^{-1})	1.94 ± 0.10	3.97 ± 0.10	3.49 ± 0.25	
*Tm*TF	ln($k_{NU}H_20$)	- 5.90 ± 0.10	-9.28 ± 0.13	-13.18 ± 1.31	-17.21 ± 1.34
	m_{NU} (M^{-1})	2.72 ± 0.04	3.21 ± 0.05	4.09 ± 0.48	4.62 ± 0.44